THE JOURNAL OF PHYSICAL CHEMISTRY LETTERS
A JOURNAL OF THE AMERICAN CHEMICAL SOCIETY

pubs.acs.org/JPCL Letter

Can a Three-Carbon Olefin Close a Five-Membered Ring on Reaction with the Silicon Nitride Radical (SiN, $X^2\Sigma^+$)? A Crossed Molecular Beams and Ab Initio Study

Surajit Metya, Daniel González, Iakov A. Medvedkov, Mateus X. Silva, Breno R. L. Galvão,* and Ralf I. Kaiser*

Cite This: *J. Phys. Chem. Lett.* 2026, 17, 4207−4213 Read Online

ACCESS | Metrics & More | Article Recommendations | Supporting Information

ABSTRACT: Substituting silicon for carbon in reactive molecular frameworks profoundly influences bonding characteristics, electronic structure, and reaction pathways, making silicon-containing systems a topic of sustained interest in fundamental and applied chemistry. Elucidating how silicon incorporation modulates elementary reaction dynamics is essential for establishing predictive principles relevant to organosilicon synthesis, materials chemistry, and heterocycle design. In this context, the reaction of the silicon nitride radical (SiN) with propene (C_3H_6) serves as an ideal model system to probe these effects. Previous studies have shown that reactions of SiN with two-carbon unsaturated hydrocarbons such as ethylene (C_2H_4) and acetylene (C_2H_2) predominantly yield acyclic silaisonitrile derivatives, whereas reactions with four-carbon systems, exemplified by 1,3-butadiene (C_4H_6), favor the formation of cyclic products. As a three-carbon unsaturated hydrocarbon, propene (C_3H_6) occupies a critical borderline position, offering a unique opportunity to determine whether silicon nitride reactivity preferentially promotes cyclic or acyclic product formation in this borderline case. Crossed molecular beam experiments, combined with high-level electronic structure calculations and Rice−Ramsperger−Kassel−Marcus (RRKM) statistical analysis, reveal that the reaction proceeds via indirect dynamics involving long-lived intermediates and tight exit transition states. Although the potential energy surface features multiple competing pathways, reaction energetics, and barrier heights strongly favor the formation of acyclic products, while cyclic Si−N heterocycles emerge only as minor channels. Together, these results provide fundamental insight into how main-group substitution governs reaction selectivity and pathway control, establishing general principles for silicon-centered reaction dynamics and expanding the conceptual framework of silicon−nitrogen chemistry.

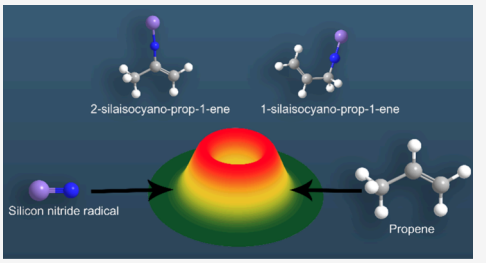

Since Langmuir introduced the concept of isoelectronicity[1] in 1919, this concept has played a central role in advancing fundamental chemical science by providing a rational framework for understanding chemical bonding and reactivity across isoelectronic systems.[2−15] A majority of the attention has been devoted to silicon chemistry, particularly in drawing comparisons with its isovalent carbon atom.[4−11] Although carbon and silicon are isovalent group 14 elements with four valence electrons, their bonding characteristics and reactivities often differ markedly. For instance, ethylene (C_2H_4) adopts a planar D_{2h} geometry, whereas disilene (Si_2H_4) favors a nonplanar, trans-bent C_{2h} structure.[16,17] A similar contrast in bonding is seen between acetylene (C_2H_2), which has a linear geometry (H−C≡C−H) with $D_{\infty h}$ symmetry, and disilyne (Si_2H_2), which favors a double-bridged "butterfly" structure [Si(μ-H_2)Si] with C_{2v} symmetry.[18] The differences in chemical reactivity are likewise pronounced: the reaction of the methylidyne radical (CH, $X^2\Pi$) with methane (CH_4) proceeds predominantly via atomic hydrogen loss to form ethylene (C_2H_4),[19] whereas the isovalent silylidyne radical (SiH, $X^2\Pi$) plus silane (SiH_4) reaction favors molecular hydrogen elimination accompanied by formation of monobridged silylidynesilylene [Si(μ-H)SiH_2] and silylsilylidyne (H_3SiSi), with the atomic hydrogen loss being endoergic by 85 kJ mol^{-1}.[20] These divergences arise from several intrinsic properties of silicon in comparison to carbon including its larger atomic radius (110 pm versus 70 pm), the lower electronegativity (1.90 versus 2.55 on the Pauling scale), the limited s−p hybridization and hence mixing between the 3s−3p orbitals in silicon versus the facile 2s−2p hybridization of carbon, and hence the reduced propensity of silicon in forming double and triple bonds.

Despite extensive comparisons between organosilicon molecules and hydrocarbons, studies focusing on silicon−

Received: January 20, 2026
Revised: March 10, 2026
Accepted: March 17, 2026
Published: March 24, 2026

https://doi.org/10.1021/acs.jpclett.6c00197
J. Phys. Chem. Lett. 2026, 17, 4207−4213

nitrogen-containing hydrocarbons and their comparison with carbon−nitrogen analogues have remained scarce. One of the promising approaches to synthesizing silicon−nitrogen hydrocarbons commences with the reaction of the silicon nitride radical (SiN, $X^2\Sigma^+$) with unsaturated hydrocarbons. Although SiN is isovalent with the cyano radical (CN, $X^2\Sigma^+$), their bonding and reactivity differ substantially. In the cyano radical, carbon and nitrogen are connected by a strong triple bond (C≡N, 117 pm, 435 kJ mol^{-1}), whereas the chemical bonding in silicon nitride is characterized by a Si═N double bond; this bond is longer (157 pm), weaker (372 kJ mol^{-1}), and significantly more polarized, leading to preferential localization of the unpaired electron on the nitrogen atom. Consequently, cyano (CN, $X^2\Sigma^+$) and silicon nitride radicals (SiN, $X^2\Sigma^+$) exhibit distinctly different reactivities. In bimolecular gas-phase reactions, organic molecules typically react with the cyano radical to form nitriles (RCN);[21] for instance, its reaction with acetylene yields cyanoacetylene (HCCCN).[22] Interestingly, isomeric isonitrile (RNC) is not formed via such gas-phase reactions at low collision energies. In contrast, Parker et al. reported that the reaction of ethylene (C_2H_4) and acetylene (C_2H_2) with the silicon nitride radical (SiN, $X^2\Sigma^+$) produces silaisocyano ethylene (C_2H_3NSi)[23] and silaisocyanoacetylene (HCCNSi), respectively.[4] An even more striking divergence is observed for reaction with 1,3-butadiene: reactions with the cyano radical yields predominantly (99%) an acyclic cyano-substituted product, 1-cyano-1,3-butadiene, via atomic hydrogen elimination,[24] whereas the silicon nitride radical predominantly forms the cyclic six-membered ring isomers (1-aza-2-silacyclohexa-3,5-dien-2-ylidene, 1-aza-2-silabenzene).[25] In this context, the reaction of the silicon nitride radical (SiN) with propene is of particular interest, as propene represents a three-carbon olefin system positioned between the two-carbon (acetylene and ethylene) and four-carbon olefin (butadiene) systems, raising the question of whether a five-membered cyclic ring is formed. Notably, two-carbon systems yield acyclic products, whereas the four-carbon system favors the formation of cyclic products.

Here, we report the reaction dynamics study of the bimolecular reaction of the silicon nitride radical (SiN, $X^2\Sigma^+$) and propene (C_3H_6, X^1A') under single collision conditions using a crossed molecular beam setup[26−33] accompanied by electronic structure calculations and a statistical analysis (Rice−Ramsperger−Kassel−Marcus, RRKM). This study demonstrates that the reaction between silicon nitride and propene predominantly yields acyclic silicon−nitrogen-containing hydrocarbons. This molecular-level investigation into the reaction dynamics between the silicon nitride radical (SiN) and propene (C_3H_6) is especially compelling from a physical-organic chemistry standpoint, as the detected products provide insight into chemical reactivity, bond dissociation pathways, and the cyclization of acyclic precursors into organosilicon rings. These findings pave the way for deeper exploration of the predominantly underexplored class of silicon−nitrogen-containing hydrocarbon molecules.

Reactive scattering signal of the bimolecular gas-phase reaction of the silicon nitride radical (SiN, $X^2\Sigma^+$; 42 amu) with propene (C_3H_6, X^1A'; 42 amu) was monitored at m/z = 83 ($SiNC_3H_5^+$), 82 ($SiNC_3H_4^+$), and 69 ($SiNC_2H_3^+$) corresponding to the atomic hydrogen loss, molecular hydrogen loss, and methyl loss, respectively. However, only the signal at m/z = 83 was observed, suggesting that the reaction proceeds predominantly through the atomic hydrogen loss channel (reaction 1). If competing H_2-loss or methyl-loss channels occur, their branching ratios must lie below the detection limit of approximately 20−30% relative to the dominant H-loss channel.

$$\mathrm{SiN(42\ amu) + C_3H_6(42\ amu) \rightarrow SiNC_3H_5(83\ amu) + H(1\ amu)} \quad (1)$$

Time-of-flight (TOF) spectra were recorded at m/z = 83 across laboratory angles ranging from 20.25° to 50.25° in 5° intervals. The TOFs were then scaled and integrated to derive the laboratory angular distribution (LAD). This LAD spans some 30° within the scattering plane defined by the intersecting beams (Figure 1) and exhibits a maximum at the center-of-mass angle of 35.25°. The symmetric nature of the LAD around the center-of-mass angle indicates that the reaction proceeds via indirect scattering dynamics, involving the formation of one or more long-lived $SiNC_3H_6$ reaction intermediates. The TOF spectra are relatively broad and display signal spread over some 300 μs ranging from 575 to 875 μs. Overall, the laboratory data provide strong evidence for the gas-phase formation of $SiNC_3H_5$ isomer(s) through the elementary reaction of silicon nitride radicals (SiN, $X^2\Sigma^+$) with propene (C_3H_6, X^1A').

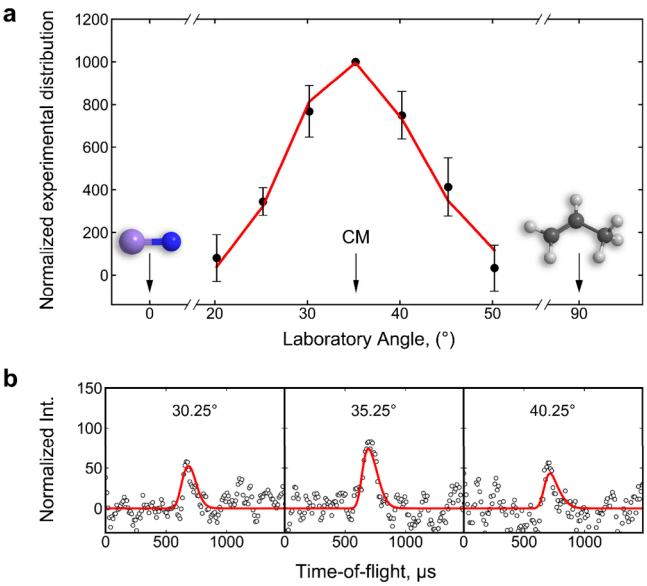

Figure 1. (a) Laboratory angular distribution and (b) time-of-flight (TOF) spectra recorded at m/z = 83 for the reaction of silicon nitride (SiN, $X^2\Sigma^+$) with propene (C_3H_6, X^1A'). In (a), the solid circles with error bars denote the normalized experimental distribution with $\pm 1\sigma$ uncertainty calculated from the standard deviation of the TOF integrals at each angle. The red lines represent the best-fit results from the forward convolution analysis. In (b), the experimental TOF data are shown as open black circles. For each angle, 1×10^6 TOF spectra (total acquisition time: 10 h) were averaged to achieve an acceptable signal-to-noise ratio, and the red line indicates the corresponding best fit.

To investigate the reaction mechanisms, a forward-convolution routine is employed to transform the laboratory data (TOFs, LAD) into the center-of-mass (CM) reference frame.[34−36] Laboratory data can be best fit with a single-channel (reaction 1) with a barrierless entrance channel. Figure

https://doi.org/10.1021/acs.jpclett.6c00197
J. Phys. Chem. Lett. 2026, 17, 4207−4213

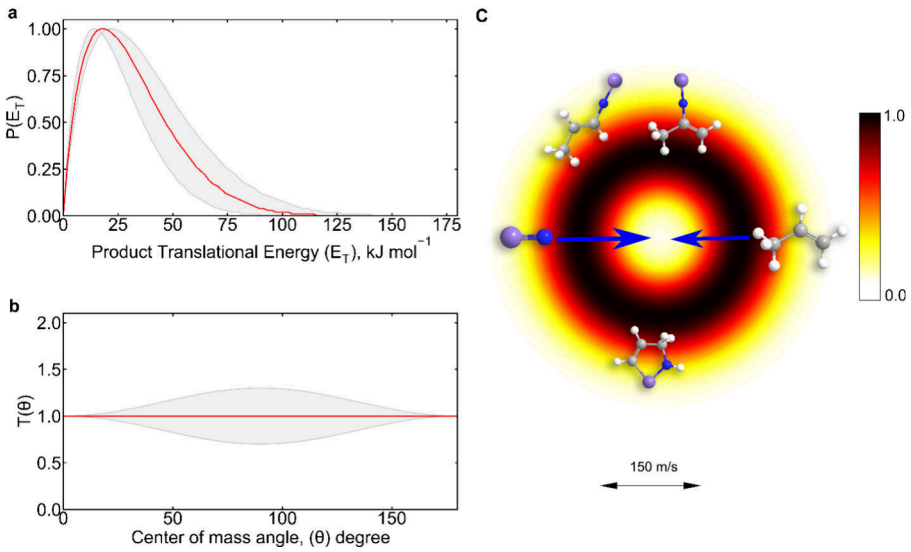

Figure 2. (a) Center-of-mass translational energy distribution $P(E_T)$, (b) the angular flux distribution $T(\theta)$, and (c) the flux contour map (top view) depicting the formation of silicon−nitrogen-containing hydrocarbon products from the reaction between ground state silicon nitride (SiN, $X^2\Sigma^+$) and propene (C_3H_6, X^1A'). The solid red lines indicate the best fit, and the shaded regions represent the error margins. The direction of the silicon nitride is defined by 0°, while that of the propene is defined at 180°. Atoms are color-coded in blue (nitrogen), violet (silicon), gray (carbon), and white (hydrogen).

2 shows the translational energy flux distribution, $P(E_T)$, and the angular flux distribution, $T(\theta)$, in the CM frame, corresponding to the best fit of the experimental data. To clarify the fundamental reaction dynamics, examining the translation energy flux distribution, $P(E_T)$, provides several important insights. First, the maximum translational energy (E_{max}) can be related to the reaction energy of the products, as E_{max} represents the sum of the reaction exoergicity and the experimental collision energy (E_c) for those molecules formed without any internal energy. The maximum translation energy for this reaction, derived from the "best" fitted experimental data, is 114 ± 25 kJ mol^{-1} (Figure 2a). By subtracting the collision energy of 22.8 ± 0.3 kJ mol^{-1}, we calculated the reaction exoergicity to be 91.2 ± 25.3 kJ mol^{-1}. Second, the peak of the translational energy distribution $P(E_T)$ at 18 ± 4 kJ mol^{-1} indicates a tight exit transition state, which is associated with significant alterations in geometry and electron density as the $SiNC_3H_6$ intermediate decomposes into the final $SiNC_3H_5$ products.[26,29,37] The angular flux distribution, $T(\theta)$, exhibits nonzero intensity across the entire angular range with a forward−backward symmetry, supporting the involvement of indirect scattering dynamics via the formation of $SiNC_3H_6$ intermediate(s) (Figure 2b). The flat $T(\theta)$ distribution suggests that the product $SiNC_3H_5$ receives substantial rotational excitation due to dissociation of intermediate $SiNC_3H_6$, and that the products are scattered in all directions with equal probability. These observations are further illustrated in the velocity−angle flux contour map (Figure 2c), which offers a comprehensive view of the scattering dynamics.

For reactions involving polyatomic species, combining experimental observations with electronic structure calculations provides a powerful approach to elucidating the underlying reaction mechanisms. Specifically, the $SiNC_3H_5$ structural isomer(s) can be identified by correlating the experimentally determined reaction exoergicity with reaction energies computed for the possible product isomers. The geometries of the relevant reactants, product isomers, intermediates, and transition states are optimized at the B2PLYP-D3(BJ)/def2-TZVPP level of theory[38−41] using ORCA,[42] and vibrational analyses were also performed at this level to obtain zero-point energies (ZPE). The energies are subsequently refined using the CCSD(T)-F12/cc-pVTZ-F12 level of theory[43−45] with an expected accuracy[46] of ±4 kJ mol^{-1} using the MOLPRO[47] software. Statistical calculations based on Rice−Ramsperger−Kassel−Marcus (RRKM) theory[48−50] were also performed to predict unimolecular reaction rate constants and product branching ratios.

The computational investigation revealed ten hydrogen loss reaction channels for silicon nitride radical (SiN) and propene (C_3H_6) system leading to distinct $SiNC_3H_5$ isomers: 1-aza-2-silacyclopenta-3-en-2-ylidene (**p1**, C_s, X^1A', −97 kJ mol^{-1}), 1-aza-2-silacyclopenta-4-en-2-ylidene (**p2**, C_s, X^1A', −94 kJ mol^{-1}), 2-silaisocyano-prop-1-ene (**p3**, C_s, X^1A', −72 kJ mol^{-1}), 1-silaisocyano-prop-1-ene (**p4**, C_s, X^1A', −62 kJ mol^{-1}), 1-silaisocyano-prop-2-ene (**p5**, C_s, X^1A', −35 kJ mol^{-1}), 1-aza-2-silacyclopenta-1,3-diene (**p6**, C_s, X^1A', −6 kJ mol^{-1}), and 1-aza-2-silacyclopenta-1,4-diene (**p7**, C_s, X^1A', −6 kJ mol^{-1}) (Figure 3). The high-energy isomers of $SiNC_3H_5$ (**p8−p10**), which are acyclic and carry a silicon−carbon bond, were not considered in constructing the potential energy surface, as they are highly endoergic and inaccessible at the experimental collision energy range (Figure 3). The calculations also identified ten intermediates (**i1−i10**) on the doublet potential energy surface, which are connected by 16 transition states (**TS1−TS16**) (Figure 4).

The computational study reveals that the reaction is initiated by a barrierless addition of the silicon nitride radical (SiN) via its radical center at the nitrogen atom to either the C2 or C1 carbon atom of propene (C_3H_6) forming the collision complexes **i1** (C_1, X^2A, −177 kJ mol^{-1}) and/or **i3** (C_1, X^2A, −178 kJ mol^{-1}); these can interconvert through a three-membered ring intermediate, **i2** (C_1, X^2A, −151 kJ mol^{-1}). From **i1**, the reaction may proceed either via isomerization to **i2** and **i3** or through hydrogen atom elimination to **p3** via an exit barrier of 29 kJ mol^{-1} above the energy of the products.

https://doi.org/10.1021/acs.jpclett.6c00197
J. Phys. Chem. Lett. 2026, 17, 4207−4213

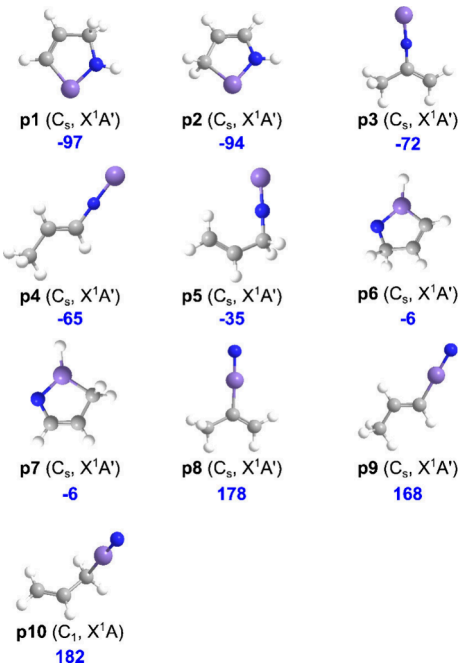

Figure 3. Optimized geometries of possible product ($SiNC_3H_5$) isomers formed in the reaction of the silicon nitride radical (SiN, $X^2\Sigma^+$) with propene (C_3H_6, X^1A'). Geometry optimizations were performed at the B2PLYP-D3(BJ)/def2-TZVPP level of theory. Point groups and electronic ground states are provided inside the parentheses. Relative energies with respect to the separated reactants, calculated at the CCSD(T)-F12/cc-pVTZ-F12 level of theory, are colored blue (kJ mol^{-1}). Atom colors denote nitrogen (blue), silicon (violet), carbon (gray), and hydrogen (white).

Apart from reverting to **i1** via **i2**, intermediate **i3** can follow three distinct pathways: atomic hydrogen elimination from C1 or C3 to yield the acyclic products **p4** and **p5** via tight exit transition states of 17 and 13 kJ mol^{-1} above the energy of the products, respectively, or isomerization to **i4** (C_1, X^2A, −173 kJ mol^{-1}) through a barrier of 168 kJ mol^{-1} above i3.

Intermediate **i4** subsequently may undergo facile ring closure to form **i5** (C_1, X^2A, −159 kJ mol^{-1}), which can then undergo either hydrogen migration from the carbon atom to nitrogen to form **i6** (C_1, X^2A, −245 kJ mol^{-1}) or hydrogen transfer from carbon to silicon, yielding **i7** (C_s, X^2A'', −152 kJ mol^{-1}). Intermediate **i6** may undergo unimolecular decomposition to the cyclic product **p1** via hydrogen atom elimination or rearrangement to **i8** (C_s, X^2A'', −219 kJ mol^{-1}) through a barrier of 188 kJ mol^{-1}. Intermediate **i8** can either decompose to **p1** by overcoming an exit transition state of 16 kJ mol^{-1} or undergo further isomerization via carbon-to-silicon hydrogen migration to **i10** (C_1, X^2A, −275 kJ mol^{-1}). Intermediate **i10** can access product **p2** via a loose exit transition state by hydrogen atom emission. On the other hand, **i7** can evolve to p6 through atomic hydrogen elimination from the C2 carbon atom, overcoming a tight exit transition state of 15 kJ mol^{-1} above the energy of the products or isomerize to **i9** (C_s, X^2A'', −126 kJ mol^{-1}) via a hydrogen shift from C2 to C3. This intermediate may form **p7** by the atomic hydrogen elimination from C1.

The most plausible reaction pathway from reactants to products can be inferred by correlating the experimental results to theoretical calculations. The experimentally determined reaction exoergicity of 91.2 ± 25.3 kJ mol^{-1} indicates the formation of at least the products **p1**−**p4**, as their calculated reaction energies fall within the corresponding experimental and computational error limits. In contrast, the calculated reaction energies for **p5**−**p7** are substantially less exoergic and can therefore be excluded as the dominating product; however, their formation might be hidden in the low-energy section of the center-of-mass translational energy distribution. Focusing on the viable channels, Figure 4 illustrates two competing pathways originating from **i1**: **i1** → **TS3** → **p3** and **i1** → **TS1** → **i2** → **TS2** → **i3**. The former pathway proceeds via a substantially higher barrier (134 kJ mol^{-1} relative to **i1**) than the latter (76 kJ mol^{-1} relative to **i1**), which leads to the

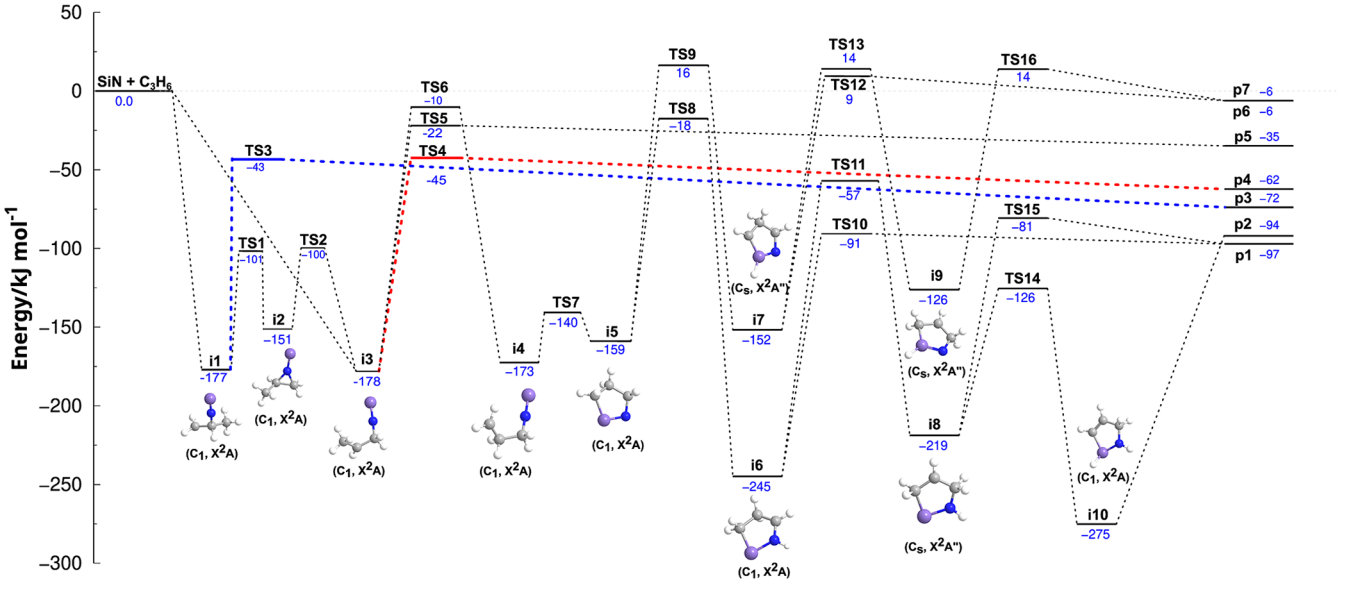

Figure 4. Potential energy surface of the reaction between the silicon nitride radical (SiN, $X^2\Sigma^+$) and propene (C_3H_6, X^1A'). Dotted lines indicate the doublet surface. Values in blue represent the energies (kJ mol^{-1}) of each species, calculated at the CCSD(T)-F12/cc-pVTZ-F12\\B2PLYP-D3(BJ)/def2-TZVPP level of theory. The dominant (red) and second-dominant (blue) pathways are highlighted.

https://doi.org/10.1021/acs.jpclett.6c00197
J. Phys. Chem. Lett. 2026, 17, 4207−4213

formation of **i3** and is therefore the more favorable path. From **i3**, pathway **i3** → **TS4** → **p4** proceeds with a lower energy barrier (133 kJ mol^{-1}) relative to **i3** than the competing path **i3** → **TS6** → **i4** (168 kJ mol^{-1}), indicating that the formation of **p4** is more preferred. Nevertheless, all intermediates and transition states lie well below the collision energy threshold, indicating that the less favored pathways proceeding via **i4** may also contribute to the formation of the cyclic product. The comparison of the competing channels **i5** → **TS8** → **i6** and **i5** → **TS9** → **i7** reveals that the former path is likely favored due to its lower barrier height (141 kJ mol^{-1} vs 175 kJ mol^{-1}) with respect to **i5**. From **i6**, between the two competing pathways **i6** → **TS10** → **p1** and **i6** → **TS11** → **i8**, the lower barrier (154 kJ mol^{-1} vs 188 kJ mol^{-1} relative to **i6**) associated with the formation of **p1** can be inferred as the preferred channel. On the other hand, **i7** predominantly leads to less exoergic products and is therefore excluded from further consideration. The distribution maximum of the center of mass translational energy distribution of 18 ± 4 kJ mol^{-1} is indicative of a tight exit transition state; consequently, the **i8** → **TS14** → **i10** → **p2** pathway, which proceeds via a loose exit transition state, can be excluded as a major contribution. Overall, the conclusive step originates from **i3**, where the transition state (**TS4**) for atomic hydrogen elimination leading to **p4** lies 35 kJ mol^{-1} lower in energy than the transition state (**TS6**) for the [1,2]-hydrogen shift from the methyl sp^3 carbon (C3) to the vinyl sp^2 carbon (C2) leading to **i4**, conferring a strong preference for formation of the acyclic product over the cyclic pathway.

To verify the most favorable reaction pathway, Rice−Ramsperger−Kassel−Marcus (RRKM) statistical analyses were performed (Supporting Information). The calculations were carried out for two distinct scenarios, starting from initial intermediates **i1** and **i3**; however, the resulting branching ratios do not differ significantly, indicating a negligible dependence on the identity of the initial intermediate. This is reflected by the fact that initially formed collision complexes **i1** and **i3** can interconvert easily via **i2**. The RRKM calculations indicate that, at the experimental collision energy, the formation of the acyclic products **p4** (83.0%) and **p3** (14.9%) dominates via **i3** → **TS4** → **p4** and **i1** → **TS3** → **p3** pathways, respectively, while only a minor contribution (0.03%) arises from the formation of the five-membered cyclic product **p1**; **p2** is not formed at all.

In summary, the reaction dynamics of the silicon nitride radical (SiN, $X^2\Sigma^+$) with propene (C_3H_6, X^1A') have been comprehensively elucidated through a synergistic combination of cross-molecular beam experiments, high-level electronic structure calculations, and RRKM statistical analysis. The experimental results demonstrate that the reaction proceeds exclusively via atomic hydrogen loss through an indirect mechanism, mediated by the formation of long-lived $SiNC_3H_6$ intermediates. Analysis of the center-of-mass translational energy distribution derived from the experimental data provides a reaction exoergicity of 91.2 ± 25.3 kJ mol^{-1}, while the observation of a peak at 18 ± 4 kJ mol^{-1} in the translational energy distribution indicates the presence of a tight exit transition state, reflecting significant structural and electronic rearrangements during product formation. Complementary high-level ab initio calculations reveal a rich potential energy surface characterized by multiple intermediates and competing reaction pathways. Correlating the computed reaction energetics with experimental observations identifies the products **p1**−**p4** as energetically accessible, whereas the less exoergic channels leading to **p5**−**p7** can be confidently excluded as the experimentally derived exoergicity constrains the energetically accessible window and disfavors the less exoergic channels. The reaction is initiated by the barrierless addition of the silicon nitride radical to propene, followed by multiple isomerization via hydrogen migrations, culminating in hydrogen-atom elimination to yield the final products. Detailed analysis of the potential energy surface further shows that the probability of formation of the acyclic products **p4** and **p3** is favored over pathways involving ring closure, although a minor contribution from the five-membered cyclic product **p1** is predicted. RRKM statistical calculations corroborate these findings, confirming that the acyclic products dominate the distribution, with branching ratios of 83.0% for **p4** and 14.9% for **p3**, while the formation of cyclic products remains a minor pathway. Overall, this study not only advances the fundamental understanding of silicon−nitrogen chemistry under isolated gas-phase conditions but also provides detailed molecular-level insight into the formation mechanisms of silicon−nitrogen-containing hydrocarbons. These findings carry broad implications for physical-organic chemistry and offer a conceptual foundation for the rational design of novel organosilicon heterocycles, bridging fundamental reaction dynamics with potential synthetic applications.

MATERIALS AND METHODS

The elementary reaction between silicon nitride radical (SiN, $X^2\Sigma^+$) and propene (C_3H_6, X^1A') was investigated in the gas phase under single-collision conditions using a crossed molecular beam apparatus. The experimental setup, data acquisition method, and analysis procedures were described in detail previously; here, we provide only a brief summary.[26−33,51] The crossed beams machine consists of a stainless-steel vacuum chamber (10^{-8} Torr) which encloses two source chambers and a triply differentially pumped ultrahigh-vacuum (10^{-12} Torr), rotatable, differentially pumped quadrupole mass spectrometric detector (QMS). A pulsed supersonic beam of silicon nitride radicals was generated *in situ* via laser ablation[30−33,51,52] of a silicon rod (Si, 99.999%, Goodfellow) at 266 nm in the presence of nitrous oxide (N_2O, 99.99%, Matheson) which released from a Proch−Trickl[53] pulsed valve (−400 V) operating at repetition rates of 60 Hz with a backing pressure of 4 atm. The rotating and translating silicon rod was ablated by focusing 2 mJ/pulse output of a Spectra-Physics Quanta-Ray Pro 270 Nd:YAG laser operating at 30 Hz. Nitrous oxide (N_2O) acted as both a reactant and a carrier gas, generating SiN radicals via nitrogen atom abstraction from N_2O by laser-ablated silicon atoms. No other silicon−nitrogen species were detected in the molecular beam. Pulsed molecular beam of the silicon nitride radical (SiN) then passed a skimmer and a four-slot chopper wheel (120 Hz), which selects a segment of the beam with a well-defined peak velocity (v_p) of 1216 ± 9 ms^{-1} and speed ratio (S) of 4.0 ± 0.1. It is important to note that the first excited state ($A^2\Pi$) of the silicon nitride radical (SiN) is located about 24 kJ mol^{-1} higher than the ground state ($X^2\Sigma^+$) and the lifetime is expected to be shorter than travel time from the ablation center to the interaction region (approximately 20 μs) as it is observed in the case of isoelectronic cyano (CN) radical whose lifetime is about 11 μs. The chopped segment of pulse silicon nitride radical (SiN) beams then crossed the pulsed molecular beam of propene (C_3H_6, 99.9%, Sigma-Aldrich) perpendicularly in the interaction region with the mean collision energy of 22.8 ± 0.3 kJ mol^{-1}. Pulsed beam of propene (60 Hz, v_p = 833 ± 15 ms^{-1}, S = 11 ± 0.1) was produced using a similar Proch−Trickl pulsed valve (−400 V), operated at a 60 Hz repetition rate with a backing pressure of 550 Torr.

Reactively scattered products were analyzed using a triply differentially pumped rotatable mass spectrometer, in which neutral species were initially ionized by an electron impact ionizer operating at 80 eV (2 mA); the resulting ions were subsequently directed into a

https://doi.org/10.1021/acs.jpclett.6c00197
J. Phys. Chem. Lett. 2026, 17, 4207−4213

quadrupole mass spectrometer (Extrel, QC 150; 2.1 MHz), where they were filtered according to their mass-to-charge ratio (m/z), before being detected by a Daly type particle ion counter[54] operated at 22.5 kV. Angularly resolved time-of-flight (TOF) spectra were recorded at discrete laboratory angles between 20.25° and 50.25°, with each spectrum instantaneously background-corrected by operating the laser at 30 Hz and the pulsed valve at 60 Hz ("laser-on" minus "laser-off"). Insight into the reaction dynamics was obtained by transforming the laboratory-frame data into the center-of-mass (CM) frame using the forward-convolution method.[34,35] This technique begins with trial center-of-mass angular flux, $T(\theta)$, and translational energy, $P(E_T)$, distributions, which are used to simulate the corresponding laboratory observables such as time-of-flight (TOF) spectra and laboratory angular distribution (LAD). These CM distributions were iteratively adjusted to achieve the best fit between the simulated and experimental TOF and LAD data. Collectively, the refined $T(\theta)$ and $P(E_T)$ distributions define the reactive differential cross section, $I(\theta, u)$, where u is the center-of-mass velocity and $I(u, \theta) \sim P(u) \times T(\theta)$. This differential cross section was ultimately visualized as a flux contour map, providing a comprehensive representation of the reaction outcome.

■ ASSOCIATED CONTENT

Supporting Information

The Supporting Information is available free of charge at https://pubs.acs.org/doi/10.1021/acs.jpclett.6c00197.

Summary of experimentally determined velocities for each reactant (Table S1), RRKM method, calculated rate constants (Table S2), calculated branching ratio (Table S3), and optimized Cartesian coordinates for each species produced in the SiN−C_3H_6 system (PDF)

■ AUTHOR INFORMATION

Corresponding Authors

Breno R. L. Galvão − *Centro Federal de Educação Tecnológica de Minas Gerais, CEFET-MG, Belo Horizonte, MG 30421-169, Brazil;* orcid.org/0000-0002-4184-2437; Email: brenogalvao@gmail.com

Ralf I. Kaiser − *Department of Chemistry, University of Hawai'i at Manoa, Honolulu, Hawaii 96822, United States;* orcid.org/0000-0002-7233-7206; Email: ralfk@hawaii.edu

Authors

Surajit Metya − *Department of Chemistry, University of Hawai'i at Manoa, Honolulu, Hawaii 96822, United States;* orcid.org/0009-0004-5583-8481

Daniel González − *Department of Chemistry, University of Hawai'i at Manoa, Honolulu, Hawaii 96822, United States*

Iakov A. Medvedkov − *Department of Chemistry, University of Hawai'i at Manoa, Honolulu, Hawaii 96822, United States;* orcid.org/0000-0003-0672-2090

Mateus X. Silva − *Centro Federal de Educação Tecnológica de Minas Gerais, CEFET-MG, Belo Horizonte, MG 30421-169, Brazil;* Present Address: Present address: Departamento de Química, Universidade Federal de Ouro Preto, Campus Morro do Cruzeiro, Ouro Preto, Minas Gerais 35402-136, Brazil; orcid.org/0000-0001-9629-3829

Complete contact information is available at: https://pubs.acs.org/10.1021/acs.jpclett.6c00197

Notes

The authors declare no competing financial interest.

■ ACKNOWLEDGMENTS

The experimental work at the University of Hawai'i at Manoa was supported by the National Science Foundation (NSF) CHE 2244717. B.R.L.G. thanks Conselho Nacional de Desenvolvimento Científico e Tecnológico (CNPq), grant 305211/2024-2.

■ REFERENCES

(1) Langmuir, I. The arrangement of electrons in atoms and molecules. *J. Am. Chem, Soc.* **1919**, *41*, 868−934.

(2) Gillespie, R. J.; Robinson, E. A. Models of molecular geometry. *Chem. Soc. Rev.* **2005**, *34*, 396−407.

(3) Kaiser, R.; Gu, X. Chemical dynamics of the formation of the ethynylsilylidyne radical (SiCCH (X Π2)) in the crossed beam reaction of ground state silicon atoms (Si (^{3}P)) with acetylene (C_2H_2 ($X^1\Sigma_g^+$)). *J. Chem. Phys.* **2009**, *131*, 104311−104316.

(4) Parker, D. S.; Wilson, A. V.; Kaiser, R. I.; Labrador, T.; Mebel, A. M. Synthesis of the Silaisocyanoacetylene Molecule. *J. Am. Chem, Soc.* **2012**, *134*, 13896−13901.

(5) Parker, D. S.; Wilson, A. V.; Kaiser, R. I.; Mayhall, N. J.; Head-Gordon, M.; Tielens, A. G. On the Formation of Silacyclopropenylidene (c-SiC_2H_2) and its Role in the Organosilicon Chemistry in the Interstellar Medium. *Astrophys. J.* **2013**, *770*, 33.

(6) Yang, T.; Dangi, B. B.; Thomas, A. M.; Sun, B. J.; Chou, T. J.; Chang, A. H.; Kaiser, R. I. Gas-Phase Synthesis of 1-Silacyclopenta-2, 4-diene. *Angew. Chem.* **2016**, *128*, 8115−8119.

(7) Yang, T.; Dangi, B. B.; Thomas, A. M.; Kaiser, R. I.; Sun, B.-J.; Staś, M.; Chang, A. H. Gas-Phase synthesis of the elusive trisilicontetrahydride species (Si_3H_4). *J. Phys. Chem. Lett.* **2017**, *8*, 131−136.

(8) Thomas, A. M.; Dangi, B. B.; Yang, T.; Kaiser, R. I.; Lin, L.; Chou, T.-J.; Chang, A. H. Are Nonadiabatic Reaction Dynamics the Key to Novel Organosilicon Molecules? The Silicon (Si (^{3}P))−Dimethylacetylene (C_4H_6 (X^1A_{1g})) System as a Case Study. *J. Phys. Chem. Lett.* **2018**, *9*, 3340−3347.

(9) Thomas, A. M.; Dangi, B. B.; Yang, T.; Kaiser, R. I.; Sun, B.-J.; Chou, T.-J.; Chang, A. H. A crossed molecular beams investigation of the reactions of atomic silicon (Si (^{3}P)) with C_4H_6 isomers (1, 3-butadiene, 1, 2-butadiene, and 1-butyne). *Chem. Phys.* **2019**, *520*, 70−80.

(10) Yang, Z.; He, C.; Goettl, S.; Kaiser, R. I. Reaction Dynamics Study of the Molecular Hydrogen Loss Channel in the Elementary Reactions of Ground-State Silicon Atoms (Si (3P)) With 1-and 2-Methyl-1, 3-Butadiene (CSH8). *J. Phys. Chem. A* **2021**, *125*, 5040−5047.

(11) Yang, Z.; He, C.; Goettl, S.; Kaiser, R. I.; Azyazov, V. N.; Mebel, A. M. Directed Gas-Phase Formation of Aminosilylene ($HSiNH_2$; X^1A'): The Simplest Silicon Analogue of an Aminocarbene, under Single-Collision Conditions. *J. Am. Chem, Soc.* **2021**, *143*, 14227−14234.

(12) Metya, S.; Goettl, S. J.; Medvedkov, I. A.; Alves, M. O.; Galvão, B. R.; Kaiser, R. I. Gas-Phase Synthesis of Germanium Monosulfide (GeS, $X^1\Sigma$+) via the Elementary Reaction of Atomic Germanium (Ge, ^{3}P) with Hydrogen Sulfide (H_2S, X^1A_1). *J. Phys. Chem. Lett.* **2025**, *16*, 4780−4787.

(13) Thomas, A. M.; Dangi, B. B.; Yang, T.; Tarczay, G. r.; Kaiser, R. I.; Sun, B.-J.; Chen, S.-Y.; Chang, A. H.; Nguyen, T. L.; Stanton, J. F. Directed Gas-Phase Formation of the Germaniumsilylene Butterfly Molecule (Ge (μ-H_2) Si). *J. Phys. Chem. Lett.* **2019**, *10*, 1264−1271.

(14) Seth, M.; Faegri, K.; Schwerdtfeger, P. The stability of the oxidation state+ 4 in group 14 compounds from carbon to element 114. *Angew. Chem., Int. Ed.* **1998**, *37*, 2493−2496.

(15) Medvedkov, I. A.; Nikolayev, A. A.; Goettl, S. J.; Yang, Z.; Mebel, A. M.; Kaiser, R. I. Experimental and theoretical study of the Sn−O bond formation between atomic tin and molecular oxygen. *Phys. Chem. Chem. Phys.* **2024**, *26*, 27763−27771.

(16) Olbrich, G. On the structure and stability of Si2H4. *Chem. Phys. Lett.* **1986**, *130*, 115−119.

(17) Dolgonos, G. Relative stability and thermodynamic properties of Si2H4 isomers. *Chem. Phys. Lett.* **2008**, *466*, 11−15.
(18) Grev, R. S.; Schaefer, H. F., III The remarkable monobridged structure of Si_2H_2. *J. Chem. Phys.* **1992**, *97*, 7990−7998.
(19) Ribeiro, J. M.; Mebel, A. M. Reaction mechanism and rate constants of the CH+ CH4 reaction: a theoretical study. *Mol. Phys.* **2015**, *113*, 1865−1872.
(20) Yang, Z.; Sun, B.-J.; He, C.; Goettl, S.; Lin, Y.-T.; Chang, A. H.; Kaiser, R. I. Combined Experimental and Computational Study on the Reaction Dynamics of the D1-Silylidyne (SiD)−Silane (SiH_4) System. *J. Phys. Chem. A* **2021**, *125*, 2472−2479.
(21) Balucani, N.; Asvany, O.; Chang, A.; Lin, S.; Lee, Y.; Kaiser, R.; Osamura, Y. Crossed beam reaction of cyano radicals with hydrocarbon molecules. III. Chemical dynamics of vinylcyanide (C_2H_3CN; X^1A') formation from reaction of CN ($X^2\Sigma^+$) with ethylene, C_2H_4 (X^1A_g). *J. Chem. Phys.* **2000**, *113*, 8643−8655.
(22) Huang, L.; Asvany, O.; Chang, A.; Balucani, N.; Lin, S.; Lee, Y.; Kaiser, R. I.; Osamura, Y. Crossed beam reaction of cyano radicals with hydrocarbon molecules. IV. Chemical dynamics of cyanoacetylene (HCCCN; $X^1\Sigma^+$) formation from reaction of CN ($X^2\Sigma^+$) with acetylene, C_2H_2 ($X^1\Sigma_g^+$). *J. Chem. Phys.* **2000**, *113*, 8656−8666.
(23) Parker, D.; Wilson, A.; Kaiser, R.; Labrador, T.; Mebel, A. Gas-Phase Synthesis of the Silaisocyanoethylene Molecule (C2H3NSi). *J. Org. Chem.* **2012**, *77*, 8574−8580.
(24) Morales, S. B.; Bennett, C. J.; Le Picard, S. D.; Canosa, A.; Sims, I. R.; Sun, B.; Chen, P.; Chang, A. H.; Kislov, V. V.; Mebel, A. M. A crossed molecular beam, low-temperature kinetics, and theoretical investigation of the reaction of the cyano radical (CN) with 1, 3-butadiene (C_4H_6). A route to complex nitrogen-bearing molecules in low-temperature extraterrestrial environments. *Astrophys. J.* **2011**, *742*, 26.
(25) Metya, S.; Medvedkov, I. A.; Goettl, S. J.; Sattasathuchana, T.; Silva, M. X.; Galvão, B. R. L.; Kaiser, R. I. One Collision − Two Heteroatoms: Gas-Phase Preparation of Azasilabenzenes. *Angew. Chem., Int. Ed.* **2026**, *65*, e17656.
(26) Kaiser, R. I. Experimental investigation on the formation of carbon-bearing molecules in the interstellar medium via neutral−neutral reactions. *Chem. Rev.* **2002**, *102*, 1309−1358.
(27) Gu, X.; Kaiser, R. I. Reaction Dynamics of Phenyl Radicals in Extreme Environments: A Crossed Molecular Beam Study. *Acc. Chem. Res.* **2009**, *42*, 290−302.
(28) Lee, Y. T. Molecular beam studies of elementary chemical processes (Nobel lecture). *Angew. Chem., Int. Ed.* **1987**, *26*, 939−951.
(29) Herschbach, D. R. Molecular Dynamics of Elementary Chemical Reactions (Nobel Lecture). *Angew. Chem., Int. Ed.* **1987**, *26*, 1221−1243.
(30) Stahl, F.; von Ragué Schleyer, P.; Bettinger, H.; Kaiser, R.; Lee, Y.; Schaefer, H., III Reaction of the ethynyl radical, C_2H, with methylacetylene, CH_3CCH, under single collision conditions: Implications for astrochemistry. *J. Chem. Phys.* **2001**, *114*, 3476−3487.
(31) Guo, Y.; Gu, X.; Kawamura, E.; Kaiser, R. I. Design of a modular and versatile interlock system for ultrahigh vacuum machines: A crossed molecular beam setup as a case study. *Rev. Sci. Instrum.* **2006**, *77*, 034701.
(32) Kaiser, R.; Chiong, C.; Asvany, O.; Lee, Y.; Stahl, F.; von, R.; Schleyer, P.; Schaefer, H., III Chemical dynamics of d1-methyldiacetylene (CH_3CCCCD; X^1A_1) and d1-ethynylallene (H_2CCCH (C_2D); X^1A') formation from reaction of C_2D ($X^2\Sigma^+$) with methylacetylene, CH_3CCH (X^1A_1). *J. Chem. Phys.* **2001**, *114*, 3488−3496.
(33) Kaiser, R.; Mebel, A.; Chang, A.; Lin, S.; Lee, Y. Crossed-beam reaction of carbon atoms with hydrocarbon molecules. V. Chemical dynamics of n-C_4H_3 formation from reaction of C (^3P_j) with allene, H_2CCCH_2 (X^1A_1). *J. Chem. Phys.* **1999**, *110*, 10330−10344.
(34) Vernon, M. F. *Molecular beam scattering*; University of California, Berkeley, 1983.
(35) Weiss, P. S. Reaction Dynamics of Electronically Excited Alkali Atoms with Simple Molecules. *Ph.D. Dissertation*; University of California, 1986.
(36) Kaiser, R. I.; Ochsenfeld, C.; Stranges, D.; Head-Gordon, M.; Lee, Y. T. Combined crossed molecular beams and ab initio investigation of the formation of carbon-bearing molecules in the interstellar medium via neutral−neutral reactions. *Faraday Discuss.* **1998**, *109*, 183−204.
(37) Levine, R. D.; Bernstein, R. B. *Molecular Reaction Dynamics and Chemical Reactivity*; Oxford University Press: Oxford, 1987.
(38) Grimme, S. Semiempirical hybrid density functional with perturbative second-order correlation. *J. Chem. Phys.* **2006**, *124*, No. 034108.
(39) Weigend, F.; Ahlrichs, R. Balanced basis sets of split valence, triple zeta valence and quadruple zeta valence quality for H to Rn: Design and assessment of accuracy. *Phys. Chem. Chem. Phys.* **2005**, *7*, 3297−3305.
(40) Becke, A. D.; Johnson, E. R. A density-functional model of the dispersion interaction. *J. Chem. Phys.* **2005**, *123*, No. 154101.
(41) Grimme, S.; Ehrlich, S.; Goerigk, L. Effect of the damping function in dispersion corrected density functional theory. *J. Comput. Chem.* **2011**, *32*, 1456−1465.
(42) Neese, F. Software update: The ORCA program system—Version 5.0. *Wiley Interdisciplinary Reviews: Computational Molecular Science* **2022**, *12*, No. e1606.
(43) Adler, T. B.; Knizia, G.; Werner, H.-J. A simple and efficient CCSD (T)-F12 approximation. *J. Chem. Phys.* **2007**, *127*, No. 221106.
(44) Knizia, G.; Adler, T. B.; Werner, H.-J. Simplified CCSD (T)-F12 methods: Theory and benchmarks. *J. Chem. Phys.* **2009**, *130*, No. 054104.
(45) Peterson, K. A.; Adler, T. B.; Werner, H.-J. Systematically convergent basis sets for explicitly correlated wavefunctions: The atoms H, He, B−Ne, and Al−Ar. *J. Chem. Phys.* **2008**, *128*, No. 084102.
(46) Zhang, J.; Valeev, E. F. Prediction of reaction barriers and thermochemical properties with explicitly correlated coupled-cluster methods: A basis set assessment. *J. Chem. Theory Comput.* **2012**, *8*, 3175−3186.
(47) Werner, H. J.; Knowles, P. J.; Knizia, G.; Manby, F. R.; Schütz, M. Molpro: a general-purpose quantum chemistry program package. *Wiley Interdisciplinary Reviews: Computational Molecular Science* **2012**, *2*, 242−253.
(48) Steinfeld, J. I.; Francisco, J. S.; Hase, W. L. *Chemical kinetics and dynamics*; Prentice Hall: Upper Saddle River, NJ, 1999.
(49) Eyring, H.; Lin, S. H. *Basic chemical kinetics*; John Wiley & Sons, Inc., 1980.
(50) Chang, A. H.; Mebel, A.; Yang, X.-M.; Lin, S.; Lee, Y. Ab initio/RRKM approach toward the understanding of ethylene photodissociation. *J. Chem. Phys.* **1998**, *109*, 2748−2761.
(51) Kaiser, R.; Hahndorf, I.; Huang, L.; Lee, Y.; Bettinger, H.; Schleyer, P. v. R.; Schaefer, H., III; Schreiner, P. Crossed beams reaction of atomic carbon, C (^3P_j), with d_6-benzene, C_6D_6 (X^1A_{1g}): Observation of the per-deutero-1, 2-didehydro-cycloheptatrienyl radical, C_7D_5 (X^2B_2). *J. Chem. Phys.* **1999**, *110*, 6091−6094.
(52) Stahl, F.; Schleyer, P. v. R.; Schaefer, H. F., Iii; Kaiser, R. I. Reactions of ethynyl radicals as a source of C_4 and C_5 hydrocarbons in Titan's atmosphere. *Planetary and Space Science* **2002**, *50*, 685−692.
(53) Proch, D.; Trickl, T. A high-intensity multi-purpose piezoelectric pulsed molecular beam source. *Rev. Sci. Instrum.* **1989**, *60*, 713−716.
(54) Daly, N. Scintillation type mass spectrometer ion detector. *Rev. Sci. Instrum.* **1960**, *31*, 264−267.

https://doi.org/10.1021/acs.jpclett.6c00197
J. Phys. Chem. Lett. 2026, 17, 4207−4213